Proceedings of
ASME TURBOEXPO 2000
May 8-11, 2000, Munich Germany

2000-GT-67

DEVELOPMENT OF CONTINUOUS FIBER REINFORCED REACTION SINTERED SILICON CARBIDE MATRIX COMPOSITE FOR GAS TURBINE HOT PARTS APPLICATION

Tsuneji Kameda, Yoshiyasu Itoh, Tsuneo Hijikata and Takanari Okamura

Power & Industrial Systems Research & Development Center,
Toshiba Corporation, Yokohama 230-0045, Japan

ABSTRACT

A dense silicon carbide matrix composite reinforced by Hi-Nicalon fibers coated with boron nitride was fabricated by slurry impregnation and subsequent reaction sintering with molten silicon. The effect of the fiber coating structure and the infiltrating metal composition on the mechanical properties of the composite was investigated. The fabrication process for the combustor liner and the shroud segment for a 15 MW gas turbine was developed. The small combustor liner and the shroud segment with some machined notches were evaluated in a combustion test at 1773 K and atmospheric pressure. Excellent durability for gas turbine hot parts was recognized.

INTRODUCTION

Ceramic matrix composite is one of the most promising candidates for high temperature structural material. SiC matrix composite is expected to be used as a material for gas turbine hot parts, because of its high temperature stability[1)-6)]. With regard to protection of fiber and interface from oxidative environment of the gas turbine, a dense matrix is favorable. Recent development of low oxygen content SiC fiber (Hi-Nicalon), which shows both excellent high temperature stability and weaving ability, makes it possible to apply various matrix consolidation processes at high temperature. Reaction sintering process is one of the suitable processes able to form a dense matrix without firing shrinkage[7)-12)].

In this work, reaction sintered SiC matrix composites reinforced by Hi-Nicalon braided fabric and uni-directional fiber were fabricated and their mechanical and fracture properties were evaluated. The combustor and shroud model parts were fabricated, and their reliability was evaluated under atmospheric pressure combustion test.

MATERIAL DEVELOPMENT

Fabrication method of composite test samples

The fabrication method for composite test samples is shown in Fig.1. Filaments of SiC fiber (Hi -Nicalon / Nippon Carbon Co., Ltd.) were coated with BN or BN/SiC by CVD. The BN and SiC coating thickness were about 0.4 μm and 0.3 μm, respectively. The fiber yarn consisted 500 filaments, and the filament diameter was about 14 μm. After 4 yarns were gathered to one fiber bundle unit, flat braided preforms made of 13 bundle units were fabricated. Or the fiber yarns were gathered uni-directionally. For the uni-directional samples, BN coating thickness of about 1.0 μm was also prepared. They were set in a porous mold and the green composites were obtained by pressure impregnating and casting of the matrix slurry. The slurry was a mixture of SiC, carbon powders and water with some dispersant. The green composites were dried and then reaction sintered at 1723 K in vacuum for 18 ks for braided samples and at 1693 K in vacuum for 0.3 ks for uni-directional samples. The infiltrating metals were 99.9 mass% purity silicon metal and 5 mass% boron doped silicon metal. The sintered bodies were machined to 1x10x40 mm test bars.

Evaluation of mechanical properties

Density and fiber volume fraction of the fabricated composite test samples were evaluated by Archimedes' method and observation of polished cross sections, respectively. The strength at room temperature was evaluated by 3-point bending test for braided samples and tensile test for uni-directional samples. The loading rates were 0.5 mm/min for bending test and 0.1 mm/min for tensile test. After the bending and tensile tests, fracture surfaces were observed by scanning electron microscope (SEM). Also fracture surfaces of pull-out fibers for

a high strength uni-directional sample were observed by SEM to evaluate in situ fiber strength via fracture mirror size.

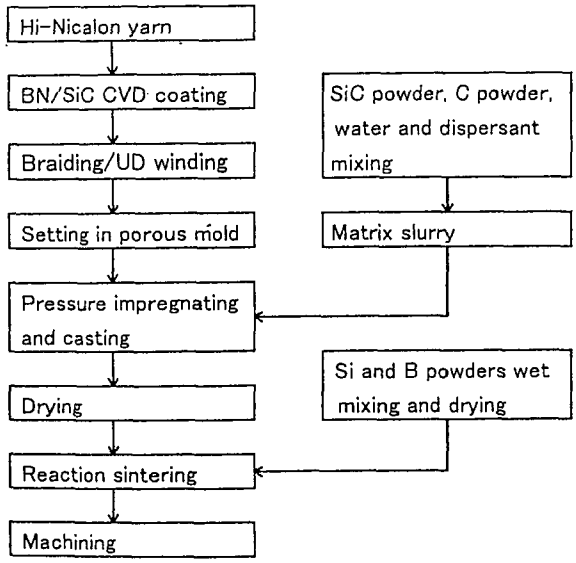

Fig.1 Flowchart of the fabrication process for the composite test samples.

Results and discussion

Density and fiber volume fraction were about 3.0 g/cm^3 and 30 vol% both for the braided and uni-directional samples.

Fig.2 shows the typical load-displacement curves for braided samples in 3-point bending test at room temperature, for BN coated fiber and Si infiltrated sample (a), for BN/SiC coated fiber and Si infiltrated sample (b), for BN coated fiber and Si-B infiltrated sample (c) and for BN/SiC coated fiber and Si-B infiltrated sample (d). Fig.3 shows SEM microphotographs of corresponding fracture surfaces. For BN coated fiber and Si infiltrated sample (a), the fracture behavior was relatively brittle. The fracture surface showed a little fiber pull-out. This was thought to be due to the degradation of the mechanical properties of the fibers, which were in contact with molten silicon during sintering. High strength and fracture energy properties were obtained for BN/SiC coated fiber and Si-B infiltrated sample (d). The fracture surface showed obvious fiber pull-out. The SiC cover coating on the BN layer was thought to be effective in preventing contact of molten silicon with the fibers, and boron doping might reduce silicon reactivity.

Fig.4 shows the ultimate strength in tensile test at room temperature for uni-directional samples with BN(0.4 μ m), BN(0.4 μ m)/SiC(0.3 μ m), BN(1.0 μ m), and BN(1.0 μ m)/SiC(0.3 μ m) coated fibers. It was clear that the ultimate tensile strength depended on the structure of the interfacial layer. The higher strengths were obtained for the coatings of thicker BN and BN/SiC structure.

Fig.5 shows the stress-strain behavior in tensile test for the sample with BN(1.0 μ m)/SiC(0.3 μ m) coated fiber. The elastic modulus was 242 GPa, and the stress increased almost linearly

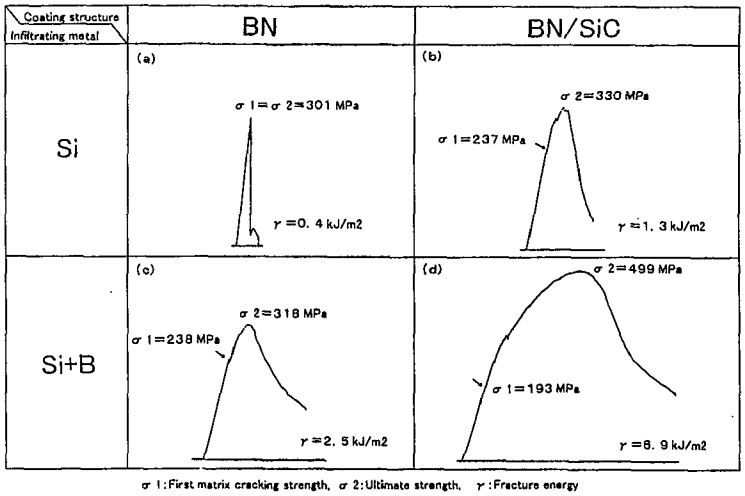

Fig.2 Typical load-displacement curves for braided samples in 3-point bending test at room temperature, for BN coated fiber and Si infiltrated sample (a), for BN/SiC coated fiber and Si infiltrated sample (b), for BN coated fiber and Si-B infiltrated sample (c) and for BN/SiC coated fiber and Si-B infiltrated sample (d).

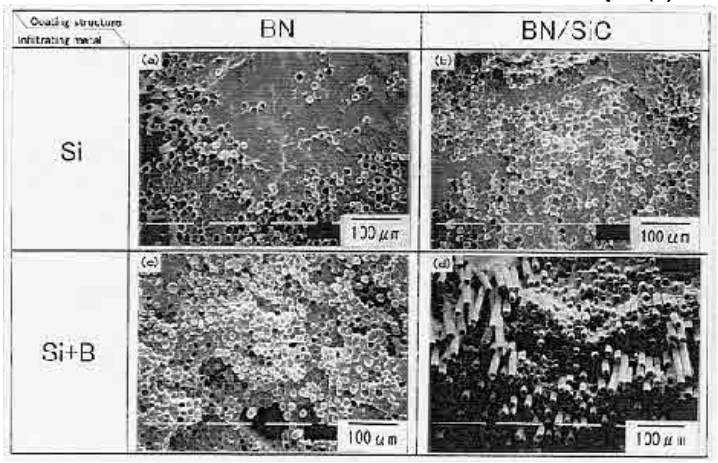

Fig.3 SEM microphotographs of fracture surfaces after 3-point bending test at room temperature, for BN coated fiber and Si infiltrated sample (a), for BN/SiC coated fiber and Si infiltrated sample (b), for BN coated fiber and Si-B infiltrated sample (c) and for BN/SiC coated fiber and Si-B infiltrated sample (d).

according to the increase of the strain up to about 400 MPa. In detail, the matrix micro-cracking was started at about 170 MPa.

For further strain increase, the stress showed a plateau. The stress increased again at around 0.4 % strain and the ultimate tensile strength of 556 MPa was reached at about 0.82 % strain. The failure elongation was about 0.93 %.

Fig.6 and 7 show SEM microphotographs of micro-cracks in the matrix and the fracture surface after tensile test. Multiple micro-cracks perpendicular to the tensile direction can be clearly observed in Fig.6. The pull-out phenomenon is more clearly shown in Fig.7.

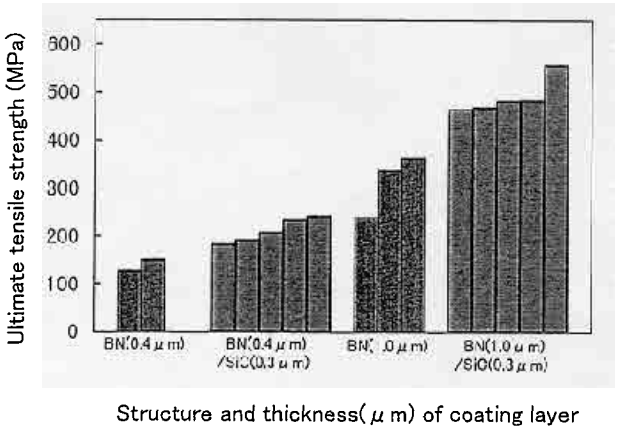

Fig.4 Ultimate strengths in tensile test for uni-directional samples with BN(0.4 μ m), BN(0.4 μ m)/SiC(0.3 μ m), BN(1.0 μ m),and BN(1.0 μ m)/SiC(0.3 μ m) coated fibers.

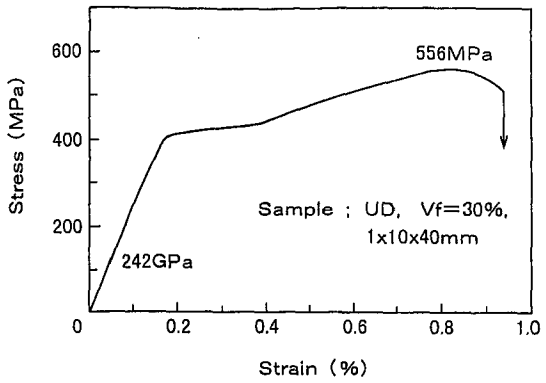

Fig.5 Typical stress-strain behavior obtained in tensile test for the uni-directional sample with BN(1.0 μ m)/SiC(0.3 μ m) coated fiber.

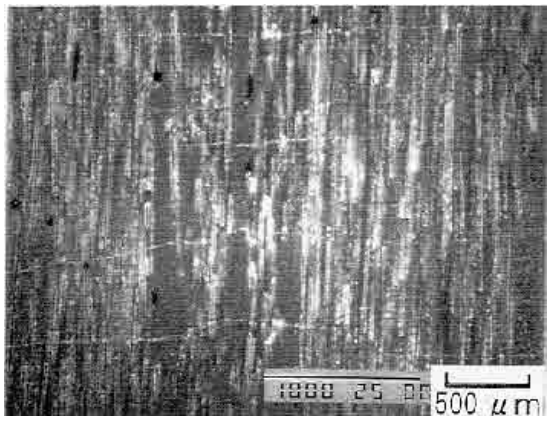

Fig.6 SEM microphotograph of micro-cracking in matrix after tensile test for the uni-directional sample with BN(1.0 μ m)/SiC(0.3 μ m) coated fiber.

To evaluate the constitutive properties of uni-directional sample, the fracture surfaces of the pull-out fibers were evaluated. In situ fiber strength was related to fracture mirror size[13]. For about 150 pieces of pull-out fibers, the fracture

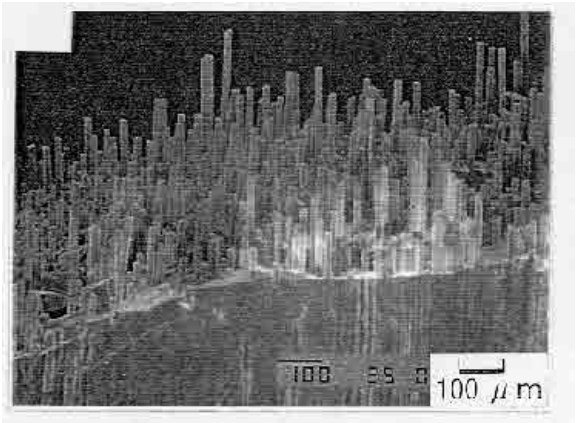

Fig.7 SEM microphotograph of fracture surface after tensile test for the uni-directional sample and fiber coated with BN(1.0 μ m)/SiC(0.3 μ m).

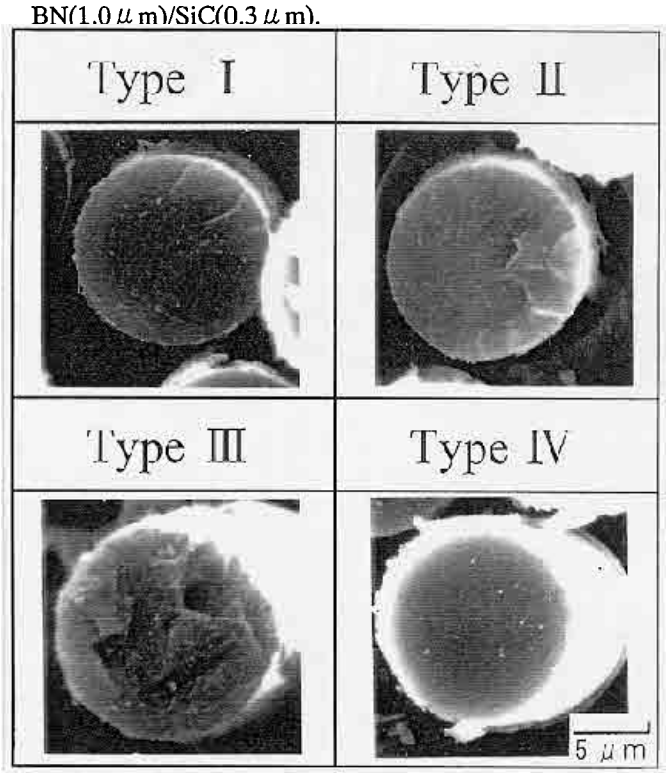

Fig.8 SEM microphotographs showing four types of fracture surfaces of pull-out fibers after tensile test (see Table 1).

surfaces were observed by SEM. The morphology of the fracture surface was divided into 4 types. Fig.8 shows typical fracture surfaces illustrating the 4 types. They were Type Ⅰ; the fracture origin was on the fiber surface and the mirror and hackle zones were distinguished, Type Ⅱ; the fracture origin was inside of the fiber and the mirror and hackle zones were distinguished, TypeⅢ; the fracture origin was unclear and the overall surface was rough, and TypeⅣ; the overall surface was flat (only mirror zone). The evaluated percentages of fracture surface types for pull-out fibers are summarized in Table 1. From the measurement of mirror radius for Type Ⅰ and Type Ⅱ,

Table 1. Observed percentage of fracture surface types for pull-out fibers

Fracture surface type	I	II	III	IV
Observed (%)	56.6	9.6	14.5	19.3

I : Fractured from surface flaw. Mirror plane observed.

II : Fractured from inner flaw. Mirror plane observed.

III : Complex fracture surface.

IV : Almost flat fracture surface.

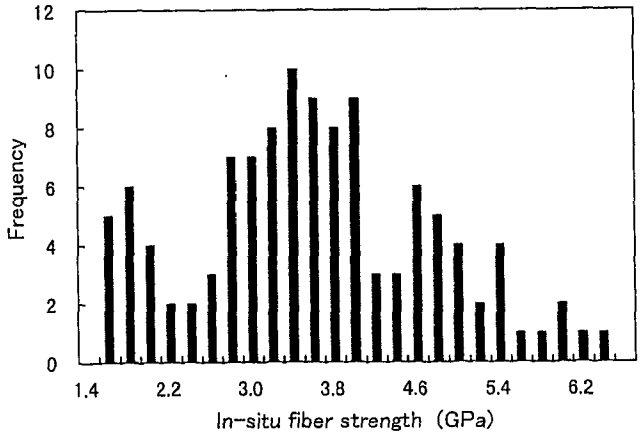

Fig.9 In situ fiber strength distribution from fracture mirror size in tensile test at room temperature.

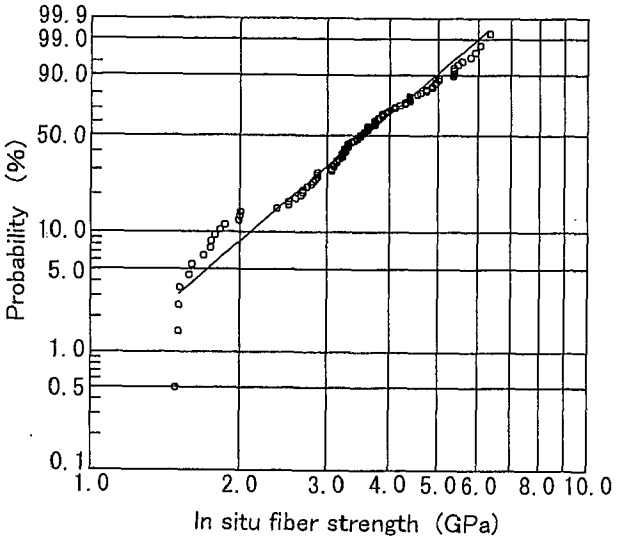

Fig.10 Weibull plot for in situ fiber strengths from fracture mirrors in composites tested in tensile mode at room temperature.

in situ fiber strengths were calculated. In this analysis, 1.48 MPa$\sqrt{m}$ was used for the K_{IC} value based on the experimental results for the relation between the tensile strength and the mirror radius of BN coated Hi-Nicalon monofilaments[14]. The in situ fiber strength distribution is shown in Fig.9. From the Weibull plot of this strength data shown in Fig.10, the values of

Table 2. Constitutive properties of uni-directional sample

Vf (%)	f 1 (%)	σ c (GPa)	m	σ uts (MPa)
30	24.2	3.87	3.65	556

Vf : Fiber volume fraction for specimen

f 1 : Effective fiber volume fraction for ultimate tensile strength

σ c : In situ fiber mean strength

m : Weibull modulus for in situ fiber strength

σ uts : Ultimate tensile strength

σc = 3.87 GPa and m = 3.65 were obtained. The fibers which failed in TypeIV mode are not thought to relate to the composite ultimate strength, because they might have failed at a lower stress level. So the effective fiber volume fraction was corrected to 30 x (1-0.193) = 24.2 %. The constitutive properties of the sample are summarized in Table 2.

GAS TURBINE HOT PARTS DEVELOPMENT

Fabrication of combustor liner and shroud segment

The combustor liner and the shroud segment were fabricated applying the same process conditions as described (d) in Fig.2 and 3. Fig.11 shows their dimensions. The combustor was small-scale and the shroud segment was full-scale for 15 MW gas turbine parts. The fiber preforms were fabricated by a filament winding technique. The fabricated parts are shown in Fig.12. As described in Fig.11, some notches were machined to evaluate crack propagation properties in the combustion test.

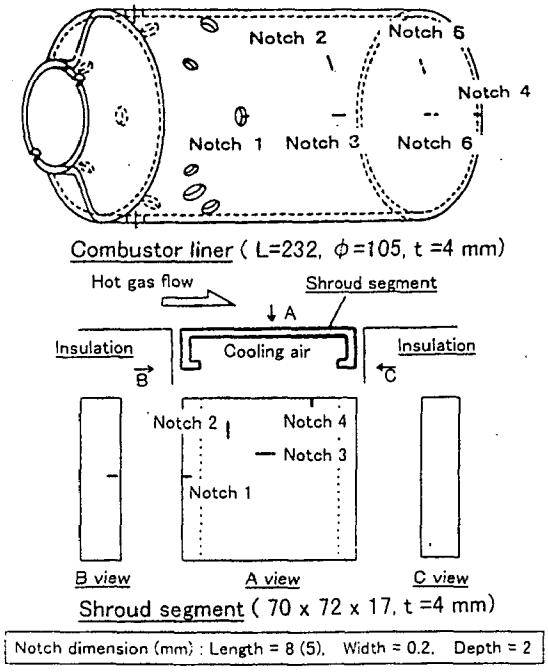

Fig.11 Combustor liner and shroud segment for combustion test.

Some properties of applied material were summarized in Table 3.

Combustor liner Shroud segment

Fig.12 Photographs of fabricated combustor liner and shroud segment.

Table 3. Material properties of combustor liner and shroud segment test parts

Material		
Fiber/matrix	SiC/SiC (Hi-Nicalon / RS-SiC)	
Fiber volume fraction Vf	30 %	
Pre-forming technique	Filament winding	
Matrix forming method	Reaction sintering	
Properties	45/-45° in plane	Through thickness
3-point bending strength (at R.T.)	First matrix cracking strength 130MPa Ultimate strength 209 MPa	
Young's modulus (at 1273K)	225 GPa	9.7 GPa
Poisson ratio (at 1273K)	0.26	0.008
Thermal conductivity (at 1273K)	30.4W/mK	16.7W/mK ,
Thermal expansion coefficient (at 1273K)	5.1x10^{-6}/K	5.4x1010^{-6}/K

Parts evaluation in combustion test

The crack propagation property for the combustor liner and the shroud segment were evaluated in the combustion thermal cycle test. Fig.13 shows the schematic illustration of the combustion test apparatus. The combustion gas was pre-heated to 673 K in the pre-combustor, then the pre-heated gas flowed to the main combustor with the test liner. At the exit of the main combustor, the hot gas path section with the test shroud segment was located. Shutting the fuel supply to the main combustor provided the thermal cycle. The fuel and air supply to the pre-combustor were constant.

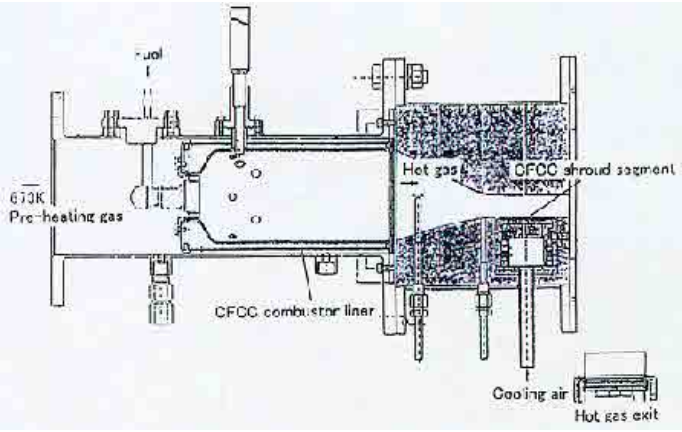

Fig.13 Schematic illustration of atmospheric combustion test apparatus.

The parts were exposed to the thermal cycle test for 51 cycles of 1573 K / 673 K for 15 min / 10 min, and subsequently 166 cycles of 1773 K / 673 K for 20 min / 10 min. The measured temperature profiles are shown in Fig.14. The temperatures were 1773 K for combustion gas and about 1473 K for the test parts. After the thermal cycle test, no crack propagation was observed at the machined notches for the combustion liner. For shroud segment, some crack propagation was observed from the notches No.1 and 4. The crack propagation from notch No.1 is shown in Fig.15. Obvious crack propagation was observed at the early stages of each test condition, but the crack propagation was saturated at higher cycle times. The microphotographs of the crack growth after 69 cycles and 132 cycles are shown in Fig.16. Photographs of the

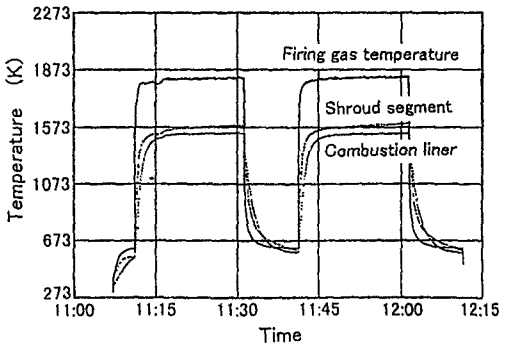

Fig.14 Temperature measurement results for 1773K combustion test.

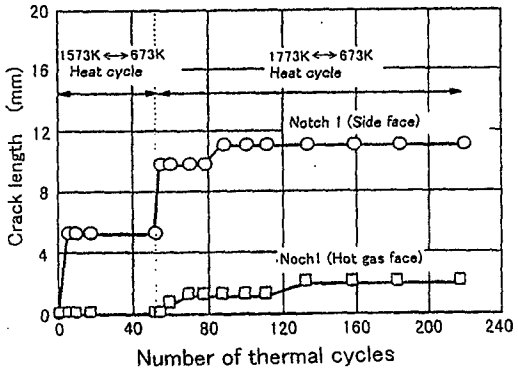

Fig.15 Crack propagation versus thermal cycles for Notch 1 of shroud segment.

Fig.16 Optical microphotographs of crack growth from Notch 1 of shroud segment after 69 and 132 thermal cycles.

shroud segment after the thermal cycle test is shown in Fig.17. Catastrophic failure was not observed at all. The tested parts show good durability.

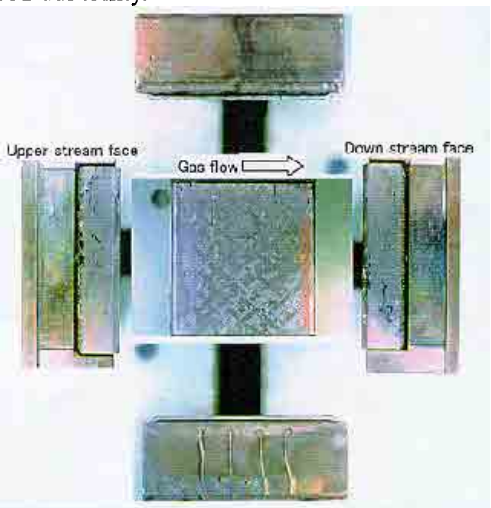

Fig.17 Photographs of shroud segment after combustion test.

FEM stress analysis

Fig.18 shows the FEM stress analysis for the shroud segment under 1773 K steady state combustion condition. The largest tensile stress was at notches No.1 and 4. In the transient analysis, about 1.2 times higher stress was observed at the same notches within 10 sec after fuel trip. This stress distribution analysis corresponds with the crack propagated locations observed in the combustion test.

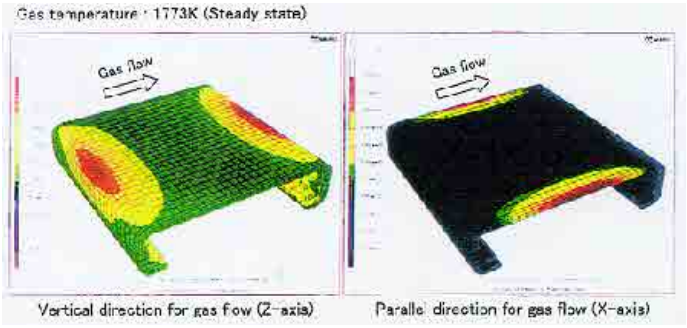

Fig.18 FEM stress analysis for the shroud segment under 1773 K steady state combustion condition

CONCLUSIONS

(1) Dense SiC matrix composite reinforced by Hi-Nicalon fibers was developed by slurry impregnation and subsequent reaction sintering process.

(2) Selecting the processing conditions of BN/SiC dual coating and Si-B metal infiltration for this composite, high strength and large fracture energy properties were achieved.

(3) The in situ fiber strength of a high tensile strength sample was evaluated from the fracture mirror size.

(4) The small-scale combustor liner and the real-scale shroud segment of 15 MW gas turbine were successfully manufactured.

(5) The crack propagation property for the combustor liner and the shroud segment were evaluated in the combustion thermal cycle test. The crack propagation was observed at the early stage of each shroud test condition, but crack propagation was saturated at higher cycle times. The tested parts show good durability.

(6) FEM stress distribution analysis corresponds with the crack propagated locations observed in the combustion thermal cycle test.

REFERENCES

1) G. S. Corman, J. T. Heinen and R. H. Goetze, ASME Paper, 95-GT-387 (1995).
2) M. H. Van de Voorde and M. R. Nedele, Ceramic Eng. & Sci. Proc., I -4, (1996) pp. 3-21.
3) K. L. Luthra, R. N. Singh and M. K. Brun, Am. Ceram. Soc. Bull., 72, 79-85 (1993).
4) A.Szweda, T. E. Easlar, D. R. Petrak and V. A. Black, ASME Paper, 99-GT-189 (1999).
5) G. S. Corman, M. K. Brun and K. L. Luthra, ASME Paper, 99-GT-234 (1999).
6) A. J. Dean, G. S. Corman, B. Bagepalli, K. L. Luthra, P. S. DiMascio and R. M. Orenstein, ASME Paper, 99-GT-235 (1999).
7) T. Kameda, A. Sayano, N. Amiji, H. Ichikawa, H. Hamada, A. Fujita, T. Uozumi, Proc. 21st An. Conf. Compos., Cocoa Beach, FL 419-26 (1997)
8) Y. Itoh, T. Kameda, K. Nishida, M. Umezawa, K. Imai, H. Ichikawa, J. Ceram. Soc. Japan, 106 [8] 830-34 (1998) [in Japanese]
9) Y. Itoh, T. Kameda, S. Suyama, K. Nagata, J. Ceram. Soc. Japan, 106 [12] 1190-95 (1998) [in Japanese]
10) T. Kameda, S. Suyama, Y. Itoh, Y. Goto, J. Ceram. Soc. Japan, 107 [4] 327-34 (1999) [in Japanese]
11) Y. Itoh, T. Kameda, S. Suyama, J. Ceram. Soc. Japan, 107 [5] 425-32 (1999) [in Japanese]
12) T. Kameda, S. Suyama, Y. Itoh, K. Nishida, J. Ceram. Soc. Japan, 107 [7] 622-26 (1999) [in Japanese]
13) R. W. Rice, "Treatise on Materials Science and Technology," Vol. II, Academic Press, New York (1978) p.199.
14) M. Umezawa (Nippon Carbon Co. Ltd.), (1998), private communication.